

Research Article



New Precursors towards the Hypergolic Synthesis of Inorganic Materials with Peculiar Morphologies

Athanasios B Bourlinos*

Abstract

Hypergolic reactions have been recently introduced from our group as a radically new preparative tool in materials science, namely hypergolic materials synthesis, allowing the fast and spontaneous synthesis of several nanomaterials at ambient conditions in an energy-liberating manner. Although the majority of the examples given from our group in this context have been mainly referred to carbon, hypergolic materials synthesis can be, in principle, extended to the synthesis of inorganic materials as well. For instance, in previous works we have illustrated that metallocenes and metallocene dichlorides in combination with fuming nitric acid HNO3 are versatile organometallic reagents towards the hypergolic synthesis of a wide range of inorganic material. In our search for additionally new precursors towards the hypergolic synthesis of inorganic materials, here we take another step-forward to show the great potential of metal (IV) dimethylamides with fuming nitric acid HNO, or of low melting point, hydrated transition metal salts (chlorides or nitrates) with sodium hydride NaH, in the synthesis of inorganic materials with peculiar morphologies through the corresponding hypergolic reactions. In particular, we show that titania TiO₂ nanoparticles with twin structure can be derived by ignition of titanium (IV) dimethylamide with fuming nitric acid HNO₃, whereas thin maghemite γ-Fe₂O₃ nanosheets by ignition of molten iron (III) chloride hexahydrate FeCl₃·6H₂O with sodium hydride NaH. The method can be equally applied to other metal (IV) dimethylamides or low melting point, hydrated transition metal salts with fuming nitric acid HNO_a or sodium hydride NaH, respectively, thus emphasizing the generality and simplicity of this new type of precursors in the hypergolic synthesis of inorganic materials.

Keywords: Fuming nitric acid; Hypergolic materials synthesis; Inorganic materials; Hydrated transition metal chlorides or nitrates; Metal(IV) dimethylamides; Sodium hydride

Introduction

Recently our group has introduced hypergolic materials synthesis as a radically new preparative technique in materials science that allows a wide range of carbon or inorganic solids with useful properties to be obtained [1-11]. Driven by simple hypergolic reactions, the new technique not only allows the fast and spontaneous synthesis of several nano-materials at ambient conditions, but also releases sizable amount of energy in the process. Despite the fact that most of the examples provided from our group involved the synthesis of carbon materials (nanosheets, nanodiscs, fluorescent carbon dots, hollow spheres, carbon nitride, graphite/ graphene and fullerols), hypergolic materials synthesis can be extended beyond carbon to include inorganic materials as well. Characteristically, in previous works we have shown the synthesis of several inorganic materials (γ -Fe₂O₂, Cr₂O₃, Co, Ni, alloy CoNi, TiO₂, ZrO₂, HfO₂, MoO₂) by the hypergolic ignition of metallocene or metallocene dichloride organometallic precursors with fuming nitric acid HNO₃ [1, 7, 11]. However, the exploration of even more chemical options in the direction of inorganic materials synthesis through hypergolic reactions still remains a challenge in order to further expand the method's portfolio of materials processing capabilities. To address this challenge, herein we exploit for the first time metal (IV) dimethylamides and low melting point, hydrated transition metal

Affiliation:

Physics Department, University of Ioannina, 45110 Ioannina, Greece

*Corresponding author:

Athanasios B Bourlinos, Physics Department, University of Ioannina, 45110 Ioannina, Greece. Tel: +302651008511.

Citation: Athanasios B Bourlinos. New Precursors towards the Hypergolic Synthesis of Inorganic Materials with Peculiar Morphologies. Journal of Nanotechnology Research 4 (2022): 111-116.

Received: July 18, 2022 Accepted: July 25, 2022 Published: July 29, 2022



salts (chlorides or nitrates) as potentially new precursors towards the hypergolic synthesis of inorganic materials with scarce morphologies. Metal (IV) dimethylamides are an important class of metalorganic compounds used extensively in chemical vapor deposition to produce thin films on various substrates. On the other hand, hydrated transition metal salts are economic and diverse starting reagents for inorganic synthesis. Indicatively here, we show that hypergolic ignition of titanium (IV) dimethylamide $Ti[N(CH_3),]_4$ by fuming nitric acid HNO₃ results in titania TiO_3 nanoparticles of twin morphology, while that of molten iron(III) chloride hexahydrate FeCl₃·6H₃O by sodium hydride NaH in thin maghemite γ-Fe₂O₂ nanosheets. The structure and morphology of the samples were verified by means of X-ray diffraction and atomic force microscopy, along with additionally 57Fe Mössbauer spectroscopy and magnetic measurements in the case of maghemite γ -Fe₂O₃. Tin (IV) dimethylamide Sn[N(CH₂)₂]₄ with fuming nitric acid HNO₂, as well as, low melting point cobalt(II) chloride hexahydrate CoCl, 6H,O and copper(II) nitrate hexahydrate Cu(NO₃)₂·6H₂O with sodium hydride NaH, are also complementary mentioned in this work in order to highlight the general use of this type of precursors in the hypergolic synthesis of inorganic materials.

Materials and Methods

All experiments were conducted with great care in a fume hood with ceramic tile bench using small quantities of reagents. Titanium(IV) dimethylamide $Ti[N(CH_3)_2]_4$ (99.999 %), tin(IV) dimethylamide $Sn[N(CH_3),]_4$ (99.9 %), iron(III) chloride hexahydrate FeCl, 6H,O (> 99 %), cobalt(II) chloride hexahydrate CoCl, 6H,O (> 99 %), copper(II) nitrate hexahydrate Cu(NO₃)₂·6H₂O (> 99 %), fuming nitric acid HNO₃ (100 %) and sodium hydride NaH (dry, 90 %) were all purchased from Sigma-Aldrich. In the case of titanium(IV) dimethylamide $Ti[N(CH_2)_2]_4$, a glass test tube was charged with 0.5 mL of the liquid reagent followed by the slow, dropwise addition of 1 mL fuming nitric acid HNO₃. Addition of the acid triggered ignition of the metalorganic precursor (Figure 1) towards the formation of titania TiO₂. The residue was successively washed with deionized water until neutral pH (e.g., fuming nitric acid HNO₃ is strongly acidic) and acetone prior to drying at 100 °C. Because the sample also contained 15 % w/w residual carbon from the metalorganic precursor, this had to be removed by calcination at 600 °C for 1 h under air. In this way, an off-white titania TiO, powder was obtained with N₂ BET specific surface area of 16 m² g⁻¹.

In the case of iron (III) chloride hexahydrate FeCl₂·6H₂O (melting point: 37 °C), 1.5 g of the transition metal salt were first melted at 100 °C inside a glass test tube. Then a total of 0.5 g of solid sodium hydride NaH were slowly added to the molten salt at small portions, causing ignition of the mixture (Figure 2) towards the formation of maghemite γ -Fe₂O₃ as the major phase. The obtained solid was successively washed with deionized water until neutral pH (e.g., sodium hydride NaH is strongly alkaline) and acetone prior to drying at 100 °C, finally affording a strongly magnetic brown powder of maghemite γ-Fe₂O₃ with N, BET specific surface area of 129 m² g⁻¹.

X-ray Diffraction (XRD) was conducted on background-free holders using Co Ka radiation from X'Pert PRO diffractometer (Malvern Panalytical) operating in Bragg-Brentano geometry. Atomic force microscopy (AFM) images were obtained in tapping mode with a Bruker Multimode 3D Nanoscope (Ted Pella Inc.) using a microfabricated silicon cantilever type TAP-300G, with a tip radius of < 10 nm and a force constant of approximately 20-75 N m⁻¹. ⁵⁷Fe Mössbauer Spectra (MS) were collected at room temperature (RT or 300 K) and 77 K using constant-acceleration spectrometers equipped with 57Co(Rh) sources kept at RT, in combination with a liquid nitrogen N, bath cryostat (Oxford Instruments Variox 760). Metallic iron α-Fe at RT was used for the velocity calibration of the spectrometers and all isomer shift (IS) values are given relative to this standard. The recorded MS were fitted using the IMSG code [12]. The magnetic properties were investigated by isothermal magnetization (M) versus applied magnetic field (H) measurements conducted at RT on a vibrating sample magnetometer (VSM) (LakeShore 7300).

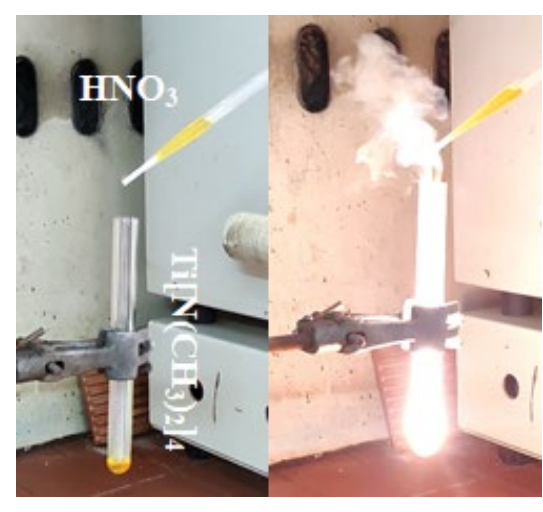


Figure 1: Hypergolic ignition of titanium (IV) dimethylamide Ti[N(CH₃)₂]₄ by fuming nitric acid HNO₃.

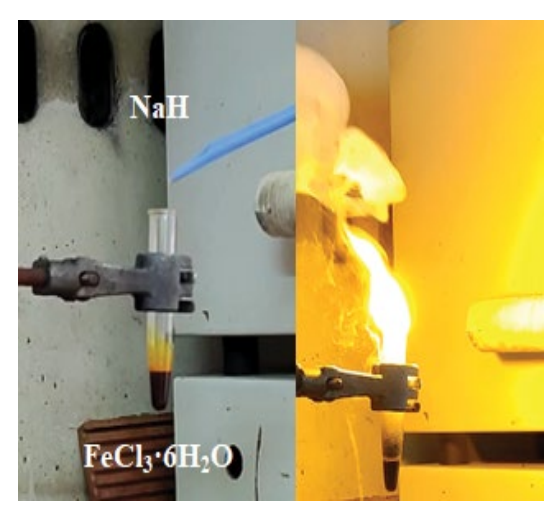


Figure 2: Hypergolic ignition of molten iron (III) chloride hexahydrate FeCl, 6H,O by sodium hydride NaH.



Results and Discussion

The hypergolic reaction between titanium (IV) dimethylamide Ti[N(CH₂)₂]₄ and fuming nitric acid HNO, towards the formation of titania TiO, can be overall described as following:

$$\underline{\text{Ti}\left[\text{N}(\text{CH}_{3})_{2}\right]_{4}} + 12 \text{ HNO}_{3} \Rightarrow \text{TiO}_{2} + 8 \text{ N}_{2} + 18 \text{ H}_{2}\text{O} + 8 \text{ CO}_{2}$$
 (1)

The XRD pattern of the as-derived titania TiO, displays characteristic diffraction peaks of the anatase and rutile phases in a ratio 70/30, based on Rietveld analysis (Figure 3). Stable anatase and metastable rutile are the two main polymorphs usually co-existing in photocatalytic titania TiO, [11]. The average particle size in the sample was estimated to be 10 nm by applying the Scherrer equation for the largest intensity diffraction peak of anatase. AFM microscopy was used in order to study the morphology of the sample (Figure 4). Accordingly, this majorly consisted of nanoparticles with twin structure and sizes in the range of 4-10 nm. These sizes are comparable to that calculated above from X-rays and the Scherrer equation. In general, nanotwinned materials have attracted great attention in recent years due to their distinctive structure [13]. At this point it is worth mentioning that the analogous liquid reagent tin (IV) dimethylamide $Sn[N(CH_3)_2]_4$ also reacts hypergolically with fuming nitric acid HNO3 to afford instead conductive stannic oxide SnO₂ (conductivity was checked by a two-point multimeter directly on the solid deposit over the glass surface of the test tube), thus overall making metal (IV) dimethylamides an important class of metalorganic precursors in the hypergolic synthesis of inorganic materials.

On the other hand, the hypergolic reaction between molten iron(III) chloride hexahydrate FeCl₃·6H₂O and sodium hydride NaH towards the formation of maghemite γ -Fe₂O₃ can be represented from the following set of reactions:

$$2 \text{ FeCl}_3 + 6 \text{ NaH} \rightarrow 2 \text{ Fe} + 6 \text{ NaCl} + 3 \text{ H}_3 \tag{2}$$

$$3 \text{ Fe} + 4 \text{ H}_2\text{O} \rightarrow \text{Fe}_3\text{O}_4 + 4 \text{ H}_2$$
 (3)

$$4 \operatorname{Fe_3O_4} + \operatorname{O_2} \rightarrow 6 \operatorname{\gamma-Fe_2O_3} \tag{4}$$

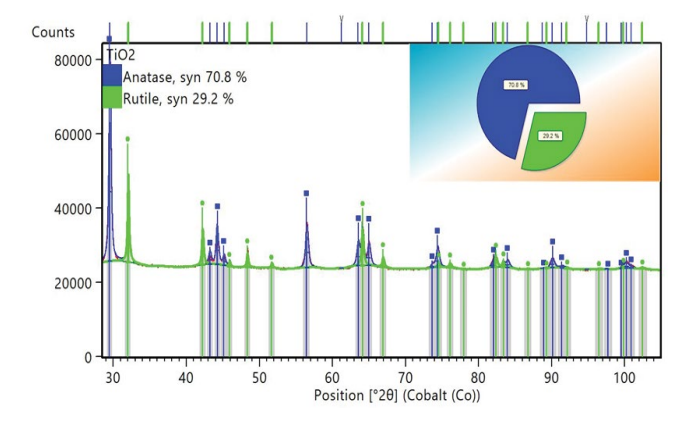


Figure 3: XRD pattern of the as-derived titania TiO, along with Rietveld analysis of the anatase and rutile phases.

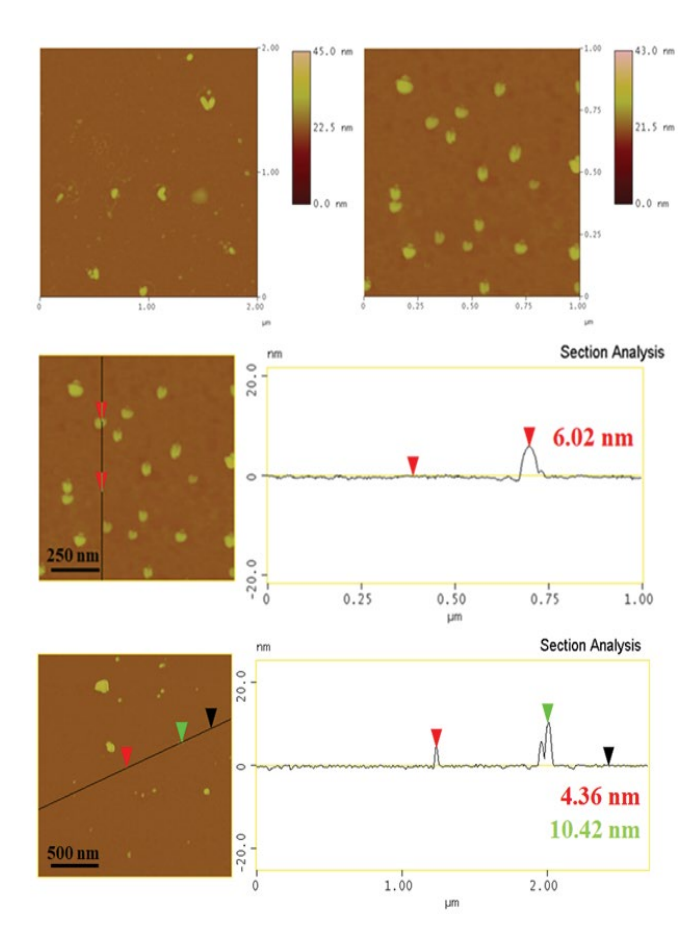


Figure 4: AFM images and corresponding height profiles of titania TiO₂ nanoparticles with twin morphology.

Where iron(III) chloride FeCl, is first reduced to metallic iron Fe by the hydride (equation 2), then the metallic iron Fe is hydrothermally converted to magnetite Fe₂O₄ (equation 3), and lastly, magnetite Fe_3O_4 is oxidized to maghemite γ - Fe_3O_3 (equation 4). The XRD pattern of the magnetic sample predominantly shows characteristic diffraction peaks from the maghemite γ-Fe₂O₃ phase (61 %), as well as from metallic iron α -Fe (13 %), hematite α-Fe₂O₃ (15 %) and goethite α-FeOOH (11 %) to a less extend (Figure 5). Metallic iron α -Fe is expected on account of equation (2), while hematite α-Fe₂O₃ and goethite α-FeOOH must be rather the byproducts of complex side reactions. Interestingly, AFM study showed mostly the presence of micron-sized thin nanosheets with thickness of 4-10 nm (Figure 6), i.e., close to the average thickness of the sheets calculated by applying the Scherrer equation for the largest intensity diffraction peak of maghemite γ -Fe₃O₃ (6 nm). The two-dimensional morphology of the sample is an intriguing result taking into consideration that the synthesis of thin maghemite γ-Fe₂O₃ nanosheets is scarce in the literature, similarly involving hydride reduction of iron(III) chloride FeCl₂ [14]. In addition, the formation of nanosheets also explains the relatively high specific surface area of the sample (129 m² g⁻¹) [14]. Besides molten iron(III) chloride hexahydrate FeCl₂·6H₂O, molten cobalt(II) chloride hexahydrate CoCl, 6H,O (melting point: 86 °C) and copper(II) nitrate hexahydrate Cu(NO₃), 6H₂O (melting point: 27 °C) react as well hypergolically with sodium



hydride to afford metallic cobalt Co and copper(II) oxide CuO, respectively, thereby suggesting that low melting point, hydrated transition metal salts are also an important source of inorganic materials through hypergolic reactions.

The presence of the above-mentioned phases in the magnetic sample was further confirmed by ⁵⁷Fe Mössbauer spectroscopy at 300 K (RT) and 77 K (liquid nitrogen) (Figure 7). The spectrum at 300 K contains contributions from a main central quadrupole split component, as well as several magnetically split components, presenting both relatively narrow as well as broad resonant lines. There are clearly two magnetically split contributions with relatively narrow resonant lines, one of which contributes its outermost lines at the highest (in absolute values) velocity scale of the absorption part of the spectrum, denoting thus a high hyperfine magnetic field (B_{hf}) value, and a second with lower B_{hf} value, but higher in absorption intensity relative to the former. We used a set of seven components to fit this spectrum, and for the broad resonant line components a spreading of B_{hf} values (ΔB_{hf}), either symmetric or asymmetric around a central B_b C value, was allowed in order to describe this broadening. The Mössbauer parameters (MPs) resulting from the best fit of this spectrum are listed in Table 1, where the greatest contribution comes from the maghemite γ -Fe₂O₃ phase.

The MPs values of the two narrow resonant line components correspond to hematite α -Fe₂O₃ (cyan) and metallic iron α -Fe (blue) phases, while contributions from other iron oxide and oxyhydroxide phases with clearly magnetically resolved resonant lines such as maghemite γ -Fe₂O₃ (brown) and goethite α -FeOOH (green) are also evident [15], in line with the XRD findings. The most broadened magnetically split components acquire MPs that are characteristic of Fe3+ high spin states in oxygen first neighbor environment. These iron oxide phases are experiencing superparamagnetic (SPM) relaxation resulting from the thermal agitation of their magnetization due to their nanosizes. The broadening of the Mössbauer resonant lines of the components corresponding to these phases comes as an effect of this relaxation, which causes the gradual collapse (COL) of their B_{hf} values [16].

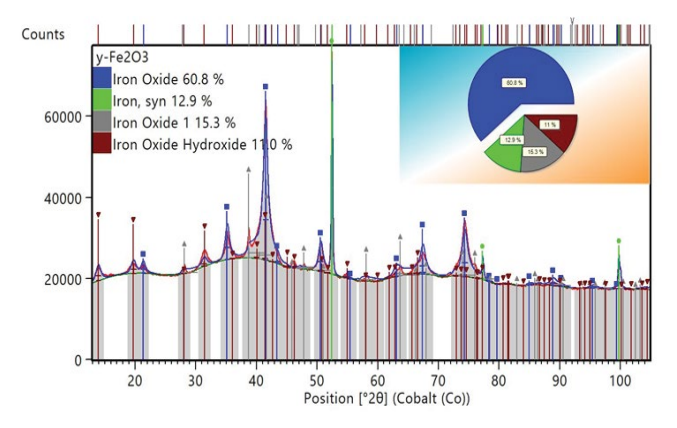


Figure 5: XRD pattern of the as-derived magnetic solid along with the Rietveld analysis of the maghemite γ-Fe₂O₃, metallic iron α-Fe, hematite α -Fe₂O₃ and goethite α -FeOOH phases.

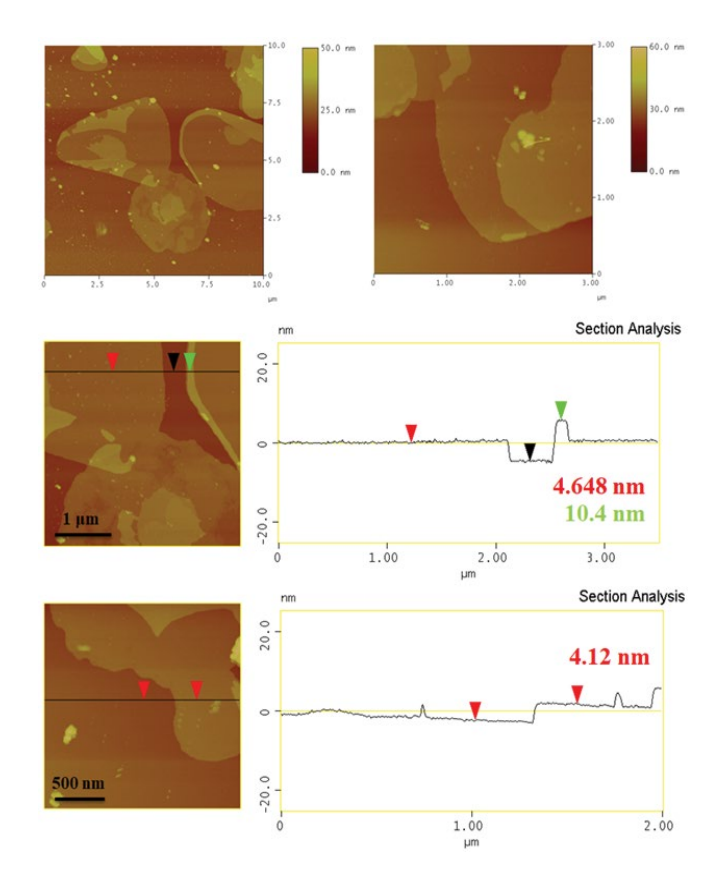


Figure 6: AFM images and corresponding height profiles of thin maghemite γ-Fe₂O₃ nanosheets.

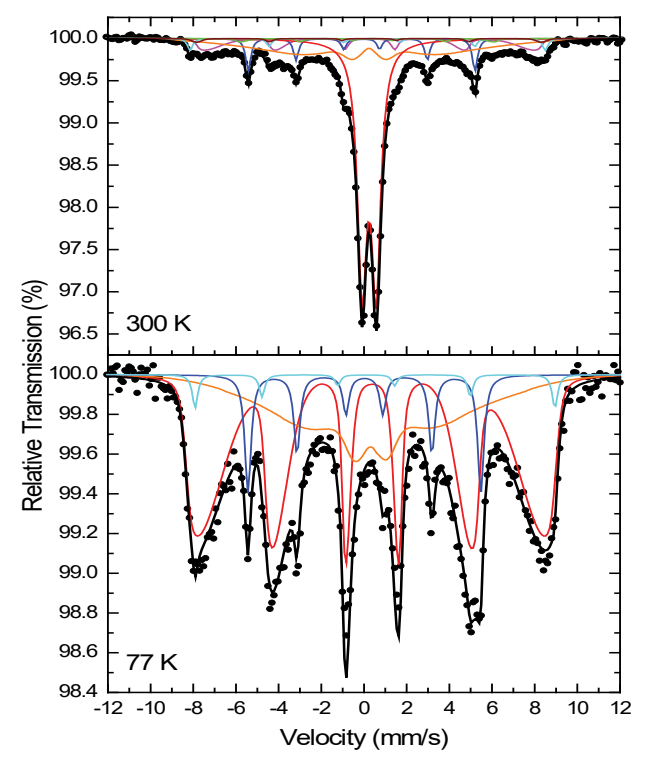


Figure 7: 57Fe Mössbauer spectra of the magnetic sample recorded at 300 and 77 K. The points correspond to the experimental data and the continuous lines to the components used to fit these spectra.



Т	IS	Γ/2	QS or 2ε	B _{hf} ^c	ΔB_{hf} or $\Delta B_{hf} < B_{hf} < \Delta B_{hf} > B_{hf}$	Area	Assignement/Color
K	mm/s	mm/s	mm/s	kOe	mm/s	%	
300	0.38	0.14	-0.20	517	1	3	Hematite/Cyan
	0.00	0.14	0.00	330	0	8	α-Fe/Blue
	0.35	0.14	-0.01	502	11	2	Maghemite/Brown
	0.38	0.14	-0.26	381	12/0	2	Goetite/Green
	0.37	0.14	-0.02	500	29/0	9	COL Maghemite/Magenta
	0.35	0.14	0.01	288	147	25	COL Maghemite /Orange
	0.35	0.26	0.66	0	0	51	SPM Maghemite/Red
77	0.42	0.15	0.41	524	0	3	Hematite/Cyan
	0.13	0.18	0.00	339	0	10	α-Fe/Blue
	0.47	0.14	-0.05	524	41/6	58	COL Maghemite-Goethite/Red
	0.54	0.14	0.24	267	117/80	29	COL Maghemite/Orange

Table 1: Mössbauer hyperfine parameters as resulting from the best fits of the corresponding spectra of the sample recorded at 300 and 77 K. IS is the isomer shift (given relative to α-Fe at 300 K), Γ/2 is the half line-width, QS is the quadrupole splitting, 2ε is the quadrupole shift, B_s is the hyperfine magnetic field, ΔB_{hr} is the spreading of B_{hr} around the central B_{hr}^{C} value (when this parameter is used) and Area is the relative spectral absorption area of each component used to fit the spectra. Typical errors are ± 0.02 mm/s for IS, Γ/2, 2ε and QS, ±3 kOe for B_n, and ± 5% for Area. In the cases where two ΔB_{hf} values are given, they correspond to asymmetric spreading around (lower/higher) the $B_{hf}^{\ \ c}$ value.

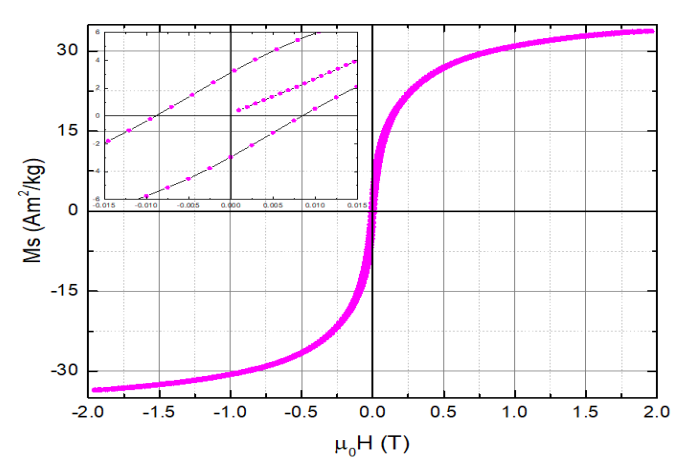


Figure 8: Magnetization vs. applied magnetic field hysteresis loop of the magnetic solid at 300 K. The inset reveals the details of the loop at low magnetic field values around zero.

Consequently, the broad resonant line components (magenta and orange) are assigned to nanomaghemite γ-Fe₂O₃ experiencing SPM relaxation. Considering a size distribution for the derived nanostructures, we can assign the part of the smaller particles in this distribution to ultrafine sized nanomaghemite γ -Fe₂O₃ for which the SPM relaxation is so fast at 300 K that their B_{hf} values collapse completely $(B_{hf} = 0)$. This group of nanostructures is represented by the quadrupole split component in the RT spectrum, which acquires also MPs characteristic of Fe³⁺ high spin states in oxygen first neighbor environment. At 77 K the thermal agitation of the magnetization for the smaller maghemite γ -Fe₂O₃ nano-objects is reduced significantly, thus the SPM component of the RT spectrum is absent at the corresponding 77 K spectrum. However, the SPM relaxation still persists at this temperature, and it is evident by the presence of two very broad magnetically split

components (red and orange) used to fit this spectrum. These components acquire the characteristic MPs of maghemite γ -Fe₂O₃ (Table 1), influenced though by the SPM relaxation (high and asymmetric ΔB_{loc} values). This large broadening screens the clear appearance of the magnetically resolved goethite α -FeOOH phase in this spectrum, however the contributions from the metallic iron α-Fe and hematite α-Fe₂O₃ phases are more evident and are included in the fitting model.

Lastly, and due to the strong magnetic character of the solid, Figure 8 presents the corresponding M vs. H loop measurement at room temperature. The contributions of the ferromagnetic metallic iron α-Fe and ferrimagnetic maghemite γ -Fe₂O₂ phases are evident from the sigmoidal shape of this loop. However, saturation of the M values is not achieved up to H=2 T, a characteristic which reflects the SPM relaxation evident by Mössbauer spectroscopy measurements. The maximum M value at H=2 T reaches $M_{max} \approx 34 \text{ Am}^2/\text{kg}$, which is lower than the nominal saturation M values of both metallic iron α -Fe (218 Am²/kg) and maghemite γ -Fe₂O₂ (76 Am²/kg) [17], revealing on the one hand the presence of the antiferromagnetic hematite α -Fe₂O₃ and goethite α -FeOOH phases in the sample, that do not contribute to M, and on the other hand the reduction of M due to SPM relaxation of the ultrafine sized nanomagnemite γ -Fe₂O₃. The coercive field reaches $H_c \approx 0.009 \text{ T (90 Oe)}$, a value which again reflects the finite size effect of the nanomaghemite γ -Fe $_2$ O $_3$ induced by their SPM relaxation.

Conclusions

Hypergolic materials synthesis defines a new preparative technique in materials science that allows the fast, spontaneous and exothermic synthesis of a wide range of nanomaterials at



ambient conditions. In this frame, our group has recently provided several examples of carbon materials syntheses but fewer ones in the direction of inorganics, the latter mainly focusing on the action of fuming nitric acid HNO₃ on organometallic precursors, such as metallocenes and metallocene dichlorides. Here special attention is given to the investigation of additional chemical options towards the hypergolic synthesis of inorganic materials with unusual shapes. The proposed alternatives include, but not limited to, (1) the hypergolic ignition of titanium (IV) dimethylamide $Ti[N(CH_2)_2]_4$ by fuming nitric acid HNO₃ towards the formation of titania TiO, nanoparticles with twin morphology, (2) the hypergolic ignition of molten iron (III) chloride hexahydrate FeCl. 6H,O by sodium hydride NaH towards the formation of thin maghemite γ -Fe₂O₃ nanosheets. Worth noting, tin (IV) dimethylamide $Sn[N(CH_3)_2]_4$ reacts similarly to titanium (IV) dimethylamide $\mathrm{Ti}[\mathrm{N}(\mathrm{CH_3})_{_2}]_{_4}$ with fuming nitric acid HNO, to correspondingly afford conductive stannic oxide SnO2, whereas cobalt (II) chloride hexahydrate CoCl, 6H,O and copper (II) nitrate hexahydrate Cu(NO₃)₂·6H₂O react similarly to iron (III) chloride hexahydrate FeCl, 6H,O with sodium hydride NaH to correspondingly afford metallic cobalt Co and copper (II) oxide CuO, respectively. Therefore, metal (IV) dimethylamides and low melting point hydrated transition metal salts (chlorides or nitrates) appear as a new and general class of precursors towards the hypergolic synthesis of inorganic materials with interesting morphologies.

Conflict of interest

The author declared that he has no conflicts of interest to this

References

- Bourlinos AB, Chalmpes N, Gournis D, et al. Hypergolic materials synthesis: a review. J Nanotechnol Res 4 (2022): 059-096.
- 2. Baikousi M, Chalmpes N, Spyrou K, et al. Direct production of carbon nanosheets by self-ignition of pyrophoric lithium dialkylamides in air. Mater Lett 254 (2019): 58-61.
- 3. Chalmpes N, Spyrou K, Bourlinos AB, et al. Synthesis of highly crystalline graphite from spontaneous ignition of in situ derived acetylene and chlorine at ambient conditions. Molecules 25 (2020): 297.

- 4. Chalmpes N, Asimakopoulos G, Spyrou K, et al. Functional carbon materials derived through hypergolic reactions at ambient conditions. Nanomaterials 10 (2020): 566.
- 5. Chalmpes N, Spyrou K, Vasilopoulos KC, et al. Hypergolics in synthesis: new paradigms and carbon nanomaterials perspectives. Molecules 25 (2020): 2207.
- 6. Chalmpes N, Tantis I, Bakandritsos A, et al. Rapid carbon formation from spontaneous reaction of ferrocene and liquid bromine at ambient conditions. Nanomaterials 10 (2020): 1564.
- 7. Chalmpes N, Bourlinos AB, Sedajova V, et al. Hypergolic materials synthesis through reaction of fuming nitric acid with certain cyclopentadienyl compounds. C 6 (2020): 61.
- 8. Chalmpes N, Bourlinos AB, Talande S, et al. Nanocarbon from rocket fuel waste: the case of furfuryl alcohol-furning nitric acid hypergolic pair. Nanomaterials 11 (2021): 1.
- Chalmpes N, Moschovas D, Tantis I, et al. Carbon nanostructures derived through hypergolic reaction of conductive polymers with fuming nitric acid at ambient conditions. Molecules 26 (2021):
- 10. Chalmpes N, Moschovas D, Bourlinos AB, et al. Hypergolic ignition of 1,3-cyclodienes by fuming nitric acid toward the fast and spontaneous formation of carbon nanosheets at ambient conditions. Micro 1 (2021): 15-27.
- 11. Chalmpes N, Asimakopoulos G, Baikousi M, et al. Hypergolic synthesis of inorganic materials by the reaction metallocene dichlorides with fuming nitric acid at ambient conditions: the case of photocatalytic titania Sci 3 (2021): 46.
- 12. Douvalis AP, Polymeros A, Bakas T. IMSG09: a ⁵⁷Fe-¹¹⁹Sn Mössbauer spectra computer fitting program with novel interactive user interface. J Phys Conf Ser 217 (2010): 012014.
- 13. Uttam P, Kumar V, Kim K-H, et al. Nanotwinning: generation, properties, and application. Mater Des 192 (2020): 108752.
- 14. Liu R, Liu J-F, Zhang L-Q, et al. Low temperature synthesized ultrathin y-Fe₂O₂ nanosheets show similar adsorption behaviour for As (III) and As(V). J Mater Chem A 4 (2016): 7606-7614.
- 15. Murad E, Jhonson JH. Iron Oxides and Oxyhydroxides. In Mossbauer Spectroscopy Applied to Inorganic Chemistry. Long GJ Ed Plenum Press: New York, USA II (1987).
- 16. Morup S. Mössbauer effect in small particles. Hyperfine Interact 60 (1990): 959-973.
- 17. Cullity BD, Graham, CD. Introduction to Magnetic Materials, Hoboken, New Jersey, John Wiley and Sons (2009).